Global vs. Local Instabilities of Pure Bcc Iron

***K. Yashiro[1] and T. Yamane[2]**

[1]Graduate School of Engineering, Kobe University, JAPAN.
[2]Former Student of Graduate School of Engineering, Kobe University, JAPAN.
*Corresponding author: yashiro@mech.kobe-u.ac.jp

Abstract

As a series study that discusses the deformation criteria based on the atomic elastic stiffness (AES), we performed various molecular dynamics simulations of perfect bulk, thin plate/wire, and tilt/twist grain boundaries (GBs) of bcc Fe. Contrary to our previous results of fcc Ni and Al, bcc Fe can reach the global instability, where all the atoms has negative AES and the system can't follow up the stress increase anymore, prior to the local deformation or nucleation of lattice defects in the tensile simulation of bulk, plate and wires. We also discuss about the negative AESs of the tilt/twist GBs against various misorientation angles for comparison with the GB energy in the no-load equilibrium. Finally we perform tensile simulations on the (322) Σ11 and (111) S3 tilt GBs ([110] tilt axis) and revealed the change in the negative AES atoms and deformation morphology.

Keywords: Local lattice instability, Atomic elastic stiffness, Surface, Grain boundary, Bcc Fe

Introduction

We considered the onset of local structural change as "local lattice instability" and attempted to find the criteria based on the atomic elastic stiffness (AES), $B_{ij}^{\alpha} = \Delta\,\sigma_i^{\alpha}/\Delta\,\varepsilon_j$, or the deformation resistance at each atom point [Yashiro and Tomita (2001)]. Here, the elastic stiffness coefficients are originally defined as the stress-strain gradient in the nonlinear elasticity [Wallace (1972)]. In the case of brittle material Si, we can observe the local to global unstable phenomena, i.e. the unstable stress drop of the whole system is triggered by the emergence of the $\det B_{ij}^{\alpha} < 0$ atoms [Yashiro and Fujihara (2011)]. On the other hand, we can't conclude which is the first, the onset of precursor deformation or the emergence of $\det B_{ij}^{\alpha} < 0$ atoms in many cases of Ni and Al [Yashiro et al. (2006), Nishimura et al. (2010)]. In the present paper, we show the relationships between the AES and the system response of bcc-Fe, derived from our investigations on the AES in bulk, at the surfaces and grain boundaries. In order to eliminate the effect of thermal vibration in this discussion, all the simulations is implemented at extremely low temperature, T=0.1K. FS potential is adopted for bcc-Fe system.

Unstable behavior of perfect bulk under [001] tension

Figure 1 shows the change in the average, standard deviation of $\det B_{ij}^{\alpha}$, and the stress-strain curve of the perfect bulk Fe under [001] tension. The bulk is represented by a cubic periodic cell of 20x20x20 unit lattices. The change in the number of $\det B_{ij}^{\alpha} < 0$ atoms is also indicated in the lower figure. The tensile simulation is implemented by usual strain control in a quasi-static manner; all the atom position is scaled according to the small strain increment, $\Delta\varepsilon_{zz}=1.0\times10^{-6}$, at each time step of 1fs. Here, the cell lengths of L_{xx} and L_{yy} are also scaled to cancel the normal stress by the Poisson's contraction. The system shows the unstable stress drop at the strain of 0.1252 due to the emergence of internal disorder or the structural relaxation as seen in the error bars of standard deviation of $\det B_{ij}^{\alpha}$; however, all the atoms already become $\det B_{ij}^{\alpha} < 0$ at the smaller strain of $\varepsilon_{zz}=0.0982$, i.e. the crystal already reached the global instability. The stress begins to decrease

after that point, resulting in the stress-peak of smooth arch, without any local change in the lattice structure. Thus the crystal would show unstable elongation under stress control tension since it couldn't follow up the stress increase anymore. We can thus conclude that the global instability is preceding to the local structural change in the bulk bcc-Fe under [001] tension. Here, we can't track what happen after the global instability since we have no answer so far for the boundary condition about the external loading due to the time-scale gap.

Unstable behavior of thin plate and wire

Then we have investigated the effect of the initial structural inhomogeneity by surfaces, preforming tensile simulations on thin plates and wires eliminating the periodic boundary condition in the normal directions against the tensile axis. Figure 2 shows the results of the (100) and (110) surface plates under the [001] tension. The right diagram of the (110) plate shows same tendency as the perfect bulk above mentioned; the stress-strain curve shows smooth

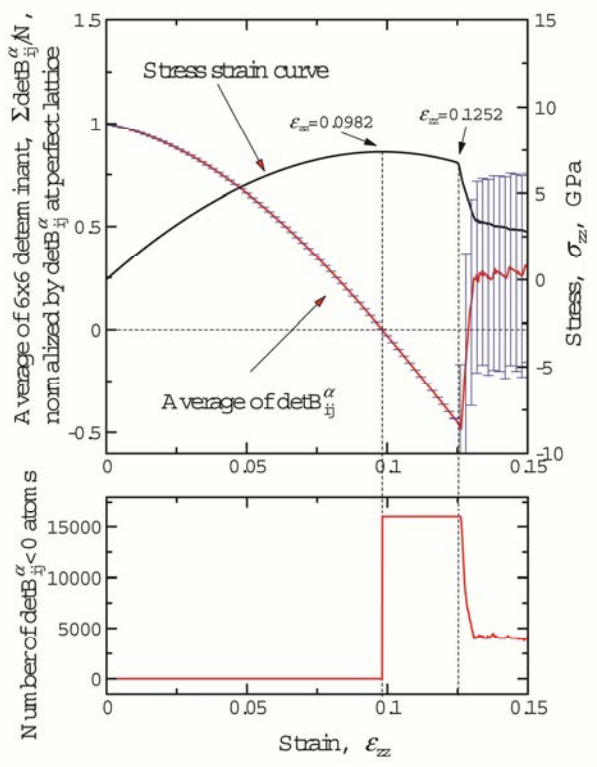

Figure 1. Change in the average of detB_{ij}^{α}, number of det$B_{ij}^{\alpha} < 0$ atoms, and the stress-strain curve of bulk Fe under [001] tension.

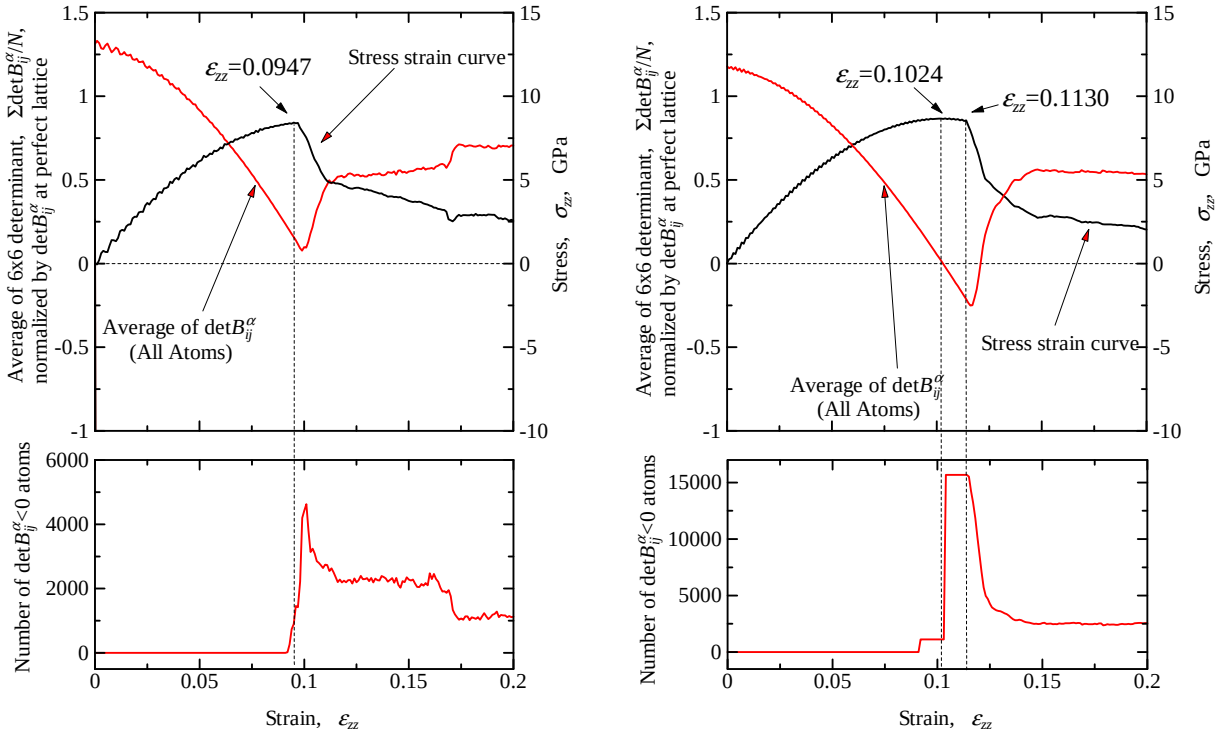

(a) (100) surface plate

(b) (110) surface plate

Figure 2. Change in the average of detB_{ij}^{α}, number of det$B_{ij}^{\alpha} < 0$ atoms, and the stress-strain curve of thin plate Fe under [001] tension.

arch and all the atoms becomes $\det B_{ij}^{\alpha} < 0$ at the peak, although the unstable stress drop by the internal structural change is observed at the later strain of ε_{zz}=0.1130. Thus we can deduce that the global instability is prior to the local deformation from the (110) surface. On the other hand, the unstable stress drop initiates at the strain of 0.0947 in the case of the (100) plate, despite of the positive value of the average of $\det B_{ij}^{\alpha}$ as often observed in fcc Ni and Al; i.e. the local deformation precedes to the global instability. The bottom of the left diagram reveals that $\det B_{ij}^{\alpha} < 0$ atoms emerge just before the stress drop and explode, then we can observe the onset of the local structural change and stress drop. Thus we can conclude that the local instability appears prior to the global one, in the case of (100) surface under the [001] tension. Both the wire models of (100)-(010) and (110)-($\bar{1}$10) surfaces also shows same tendency, that is, the local structural change occurs from the surfaces before the global instability point. On the other hand, in the case of the [$\overline{1}\overline{1}$2] tension, both the thin plate of (111) surface and the wire of (111)-($\bar{1}$10) surfaces shows the stress drop after the global instability or the smooth stress peak; thus we can deduce that the surfaces are not potential candidate of the local deformation, under the [112] tension of bcc Fe.

Atomic elastic stiffness of symmetrical tilt/twist grain boundaries

Figure 3 illustrates the number of $\det B_{ij}^{\alpha} < 0$ atoms and the grain boundary (GB) energy per unit area against the misorientation angle of the [110] tilt and the [001] twist GBs. Here infinite laminate structures of GBs are assumed under the periodic boundary conditions. The size of the simulation cells is different for each GBs due to the coincidence site lattice (CSL) so that we don't discuss about the averages of $\det B_{ij}^{\alpha}$. We may recognize same analogy between negative atoms and GB energy, e.g. there is no $\det B_{ij}^{\alpha} < 0$ atoms on the (112) Σ3 tilt and Σ3 twist GBs, which are well-known stable GBs as can be seen in the energy cusp. However, the number of $\det B_{ij}^{\alpha} < 0$ atoms shows more complicated change, contrast to the rather monotonic change of GB energy. For example, the (332) Σ11 tilt GB has many negative $\det B_{ij}^{\alpha}$ atoms despite of the energy cusp, while the (111) Σ3 tilt GB has few $\det B_{ij}^{\alpha} < 0$ atoms although there is no remarkable cusp in the GB energy curve.

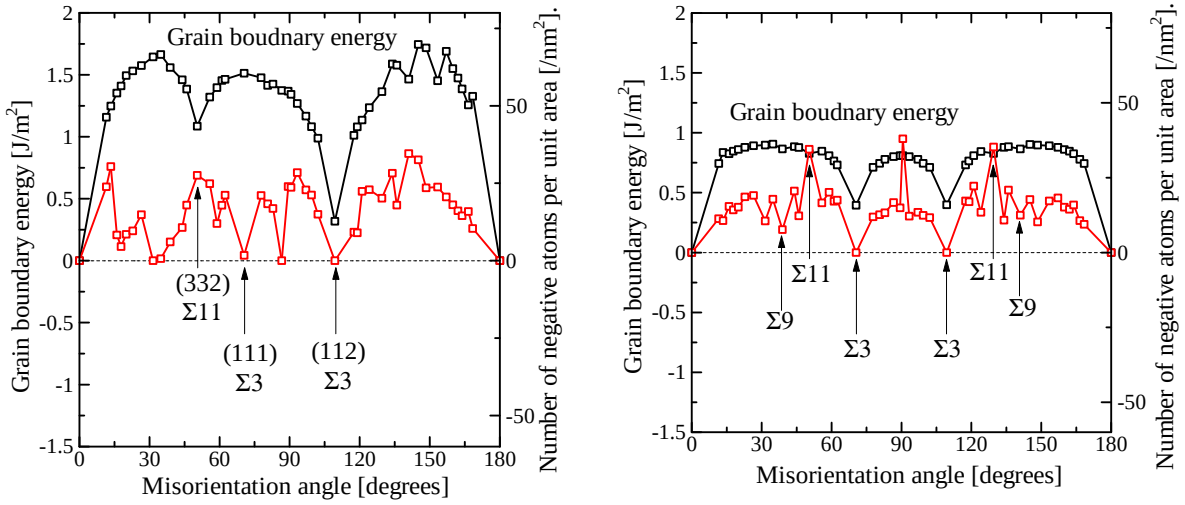

(a) [110] tilt G.B. (b) [001] twist G.B.

Figure 3. Relationships between grain boundary energy and misorientation angle, and the ratio of negative $\det B_{ij}^{\alpha}$ atoms.

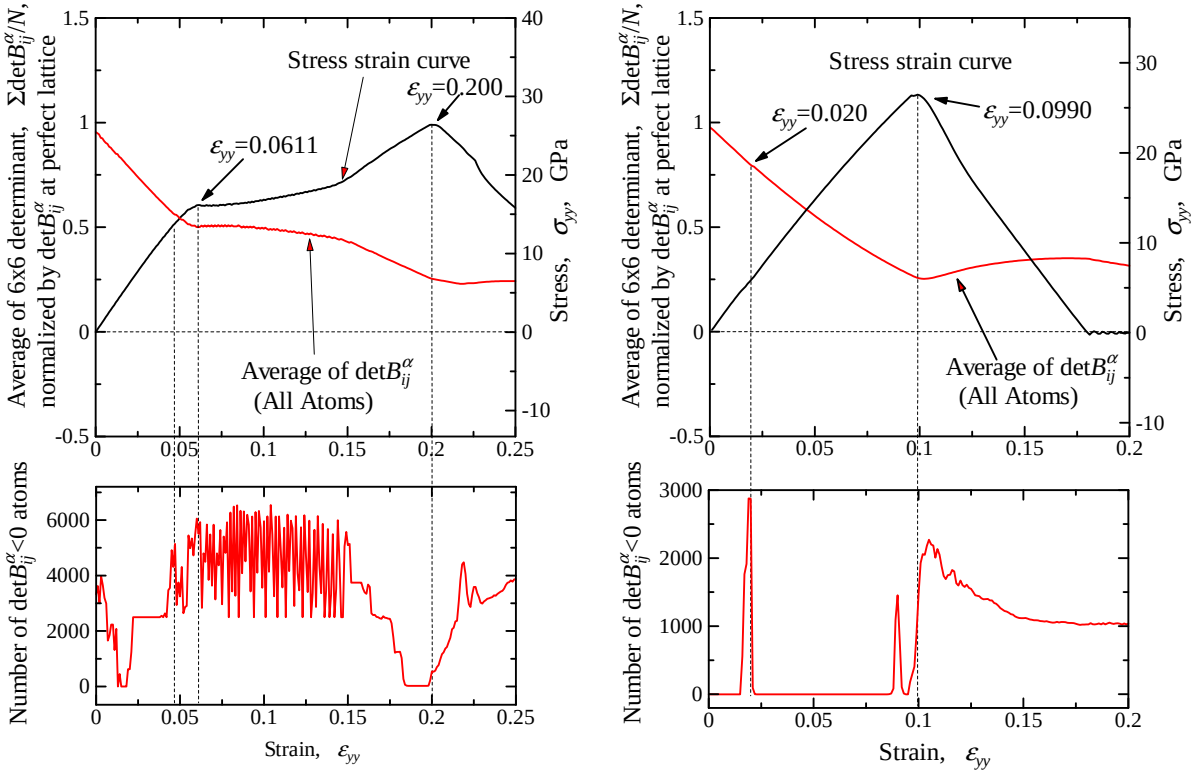

(a) (332) Σ11 tilt G.B. (b) (111) Σ3 tilt G.B.

Figure 4. Stress-strain curve, the change in the average of $\det B_{ij}^{\alpha}$ and the number of $\det B_{ij}^{\alpha}$<0 atoms under tension (infinite laminate structure of tilt GBs).

We then performed tensile simulations on the (332) Σ11 and the (111) Σ3 tilt GBs, in the direction normal to the GB plane (*y*-axis). Here we didn't control the Poisson's contraction or the lateral strain ε' is fixed at zero during the simulations. The simulation results are summarized in Fig.4. As already indicated in Fig.3, the (332) Σ11 tilt GB has many negative atoms at the initial equilibrium; however, the negative atoms decrease and finally vanish by the external load during ε_{yy}=0~0.015, although there is no remarkable change in the stress-strain curve. Then atoms on the layers just above and below the GB planes become negative at the strain of 0.022, as recognized with the similar snapshot at ε_{yy}=0.0474 in Fig.5. The stress-strain curve shows the remarkable blunting of stress increase at ε_{yy}=0.0611. Figure 5 shows the internal change during the blunting-plateau response by the sign of $\det B_{ij}^{\alpha}$ and central symmetry parameter of Atomeye [Li (2003)]. The bcc-bct phase transition occurs from the GB and propagates in the grains, finally the bct phase covers whole the grains. We can find the negative AES atoms at the forward edge of the expanding phase, or at the migrating boundary. The strain hardening at the later stage is caused by this phase transition. The crystal shows the highest peak at ε_{yy}=0.200 where a cleavage cracking emerges at the new boundary seen in the snapshot at ε_{yy}=0.151 in Fig.5. On the other hand, the stable (111) Σ3 tilt GB doesn't show GB migration but cleavage cracking at the first and highest peak of ε_{yy}=0.099, after showing pulse-like pop-up of negative AES atoms at ε_{yy}=0.020 and ε_{yy}=0.090. The negative AES atoms can be seen only at the GB as shown in Fig.6. From the GB energy at the initial equilibrium, the (111) Σ3 tilt GB is considered more stable than the (322) Σ11 one. In fact, the magnitude relation of the stress and strain of the first peak obeys this prediction; however, the later has deformability and shows better ductility than the former.

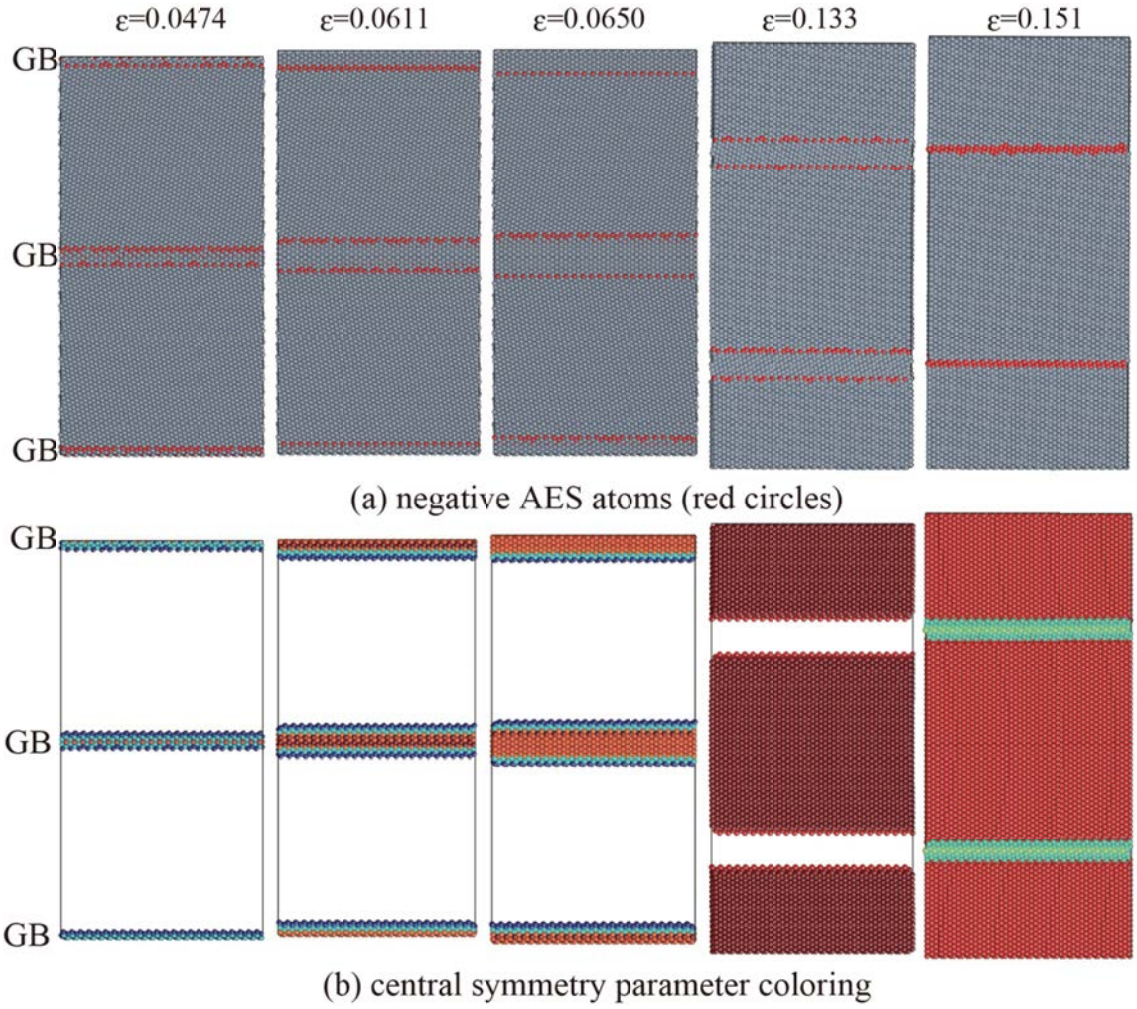

Figure 5. Snapshots of (332) Σ11 symmetric tilt grain boundary under tension

Conclusions

In the present paper, we performed various primitive simulations on bcc Fe to reveal the characteristics of the atomic elastic stiffness (AES) in the perfect bulk, thin plate/wires, tilt/twist grain boundaries (GBs). It is remarkable difference from our previous results of fcc Ni/Al and diamond lattice of Si, that bcc Fe can reach the global instability prior to the local deformation or nucleation of lattice defects in the tensile simulation of bulk, plate and wires. Here, the global instability means all the atoms has negative AES and the system can't follow up the stress increase anymore against external loading. We also investigated the negative AES per unit area against various misorientation angles of tilt/twist grain boundaries, comparing with the GB energy diagram. We also performed tensile simulations on the (322) Σ11 and (111) Σ3 tilt GBs ([110] tilt axis) and revealed that the later actually shows higher elastic limit than the former as predicted by the GB energy before loading; however, the former shows better ductility due to the phase transformation from GBs after the elastic limit, while the later immediately fractured at the GB by cleavage cracking. It is still difficult to connect the stress-strain response to the change in the negative AES, however, it should be noted that we have observed the negative AES at the front edge of the propagating boundary of the phase transformation.

References

Li J. (2003) AtomEye: an Efficient Atomistic Configuration Viewer, *Modelling Simul. Mater. Sci. Eng.* Vo.11, pp.173-177.

Nishimura, M., Yashiro, K. and M. Arai (2010) Local Lattice Instability Analysis on Amorphous Metals: Stability Switching between Stable and Unstable, *Journal of Solid Mechanics and Materials Engineering*, Vol.4, No.11, pp.1550-1562.

Wallace, D. C. (1972) *Thermodynamics of Crystals*, Newyork.

Yashiro, K. and Tomita, Y (2001) Local Lattice Instability at a Dislocation Nucleation and Motion, *Journal de Physique* IV, 11, Pr5-3－Pr5-10, EDP Sciences.

Yashiro, K. Nishimura, M. and Tomita, Y. (2006) Deformation Analysis of Amorphous Metals Based on Atomic Elastic Stiffness Coefficients, *Modelling and Simulation in Materials Science and Engineering*, Vol.14, pp.597-605.

Yashiro, K. and M. Fujihara (2012) Molecular dynamics study on atomic elastic stiffness in Si under tension: homogenization by external loading and its limit, *Modelling and Simulation in Materials Science and Engineering*, Vol. 20, No. 4, 045002.

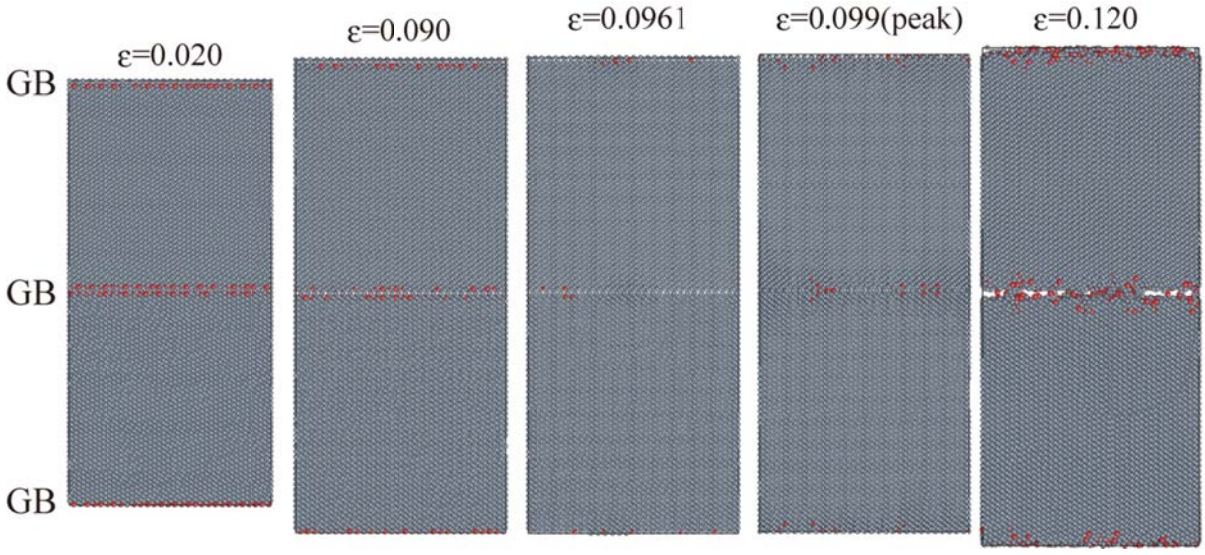

Figure 6. Snapshots of (111) Σ3 symmetric tilt grain boundary under tension. Red circles indicate negative AES atoms.